Table of Contents

Updated / Edited by	Approved
Specialist Committee on Uncertainty Analysis of 25th ITTC	25th ITTC 2008
Date 2008	Date 09/2008

Uncertainty Analysis: Particle Imaging Velocimetry (PIV)

1. PURPOSE OF PROCEDURE

The purpose of this procedure is to describe the method for uncertainty analysis on flow field measurement by means of particle image velocimetry (PIV). An example of uncertainty analysis (UA) procedure is presented, and it shows typical propagation of measurement uncertainties in PIV measurement.

2. SCOPE

The PIV measurement system consists of several sub-systems, and the evaluation of the measurement needs to consider the coupling between the sub-systems. The guideline of UA on PIV measurement has been proposed by the Visualization Society of Japan (VSJ, 2002) as a result of an organized project on PIV standardization (PIV-STD project, Nishio, et al., 1999). The present procedure was developed based on the guideline of VSJ recommendation. The present procedure is limited to the PIV measurement itself. The uncertainties of model test are not included. The total evaluation of the experiment should consider the contribution of model test uncertainty separately.

3. GENERAL

The PIV measurement detects the flow speed by means of the displacement of particle images ΔX, and the time interval of successive images Δt. The magnification factor α needs to be identified through the calibration, and it provides the physical amount of flow speed. The PIV measurement based on the visualized flow image, and the information of the image differs from the flow field due to the velocity lag of the tracer particle from acceleration and the projection procedure from the 3-D physical space to 2-D image plane. These uncertainty factors of flow visualization are consolidated in a parameter δu. The δu is generally hard to detect systematically generally, and it is usually categorized as an uncertainty factor rather than a measurement parameter. The principle of the PIV measurement on flow speed u can be described by Equation (1).

$$u = \alpha(\Delta X/\Delta t) + \delta u \tag{1}$$

The PIV measurement system detects the displacement of particle image by means of the correlation of particle pattern in successive particle image. The image analysis of PIV started from the auto-correlation technique, which uses double exposed particle image (Adrian, 1986). It was expanded to the cross-correlation analysis (Kimura, et al., 1986, Keane, et al., 1991), and most commercial PIV systems are based on it. The correlation between successive particle images $f(X, Y)$, $g(X, Y)$ is evaluated by the correlation coefficient shown by Equation (2), and the normalized form shown by Equation (3) is usually used. The f_m and g_m and in Equation (3) show the averaged luminance value of correlation area. The maximum value of correlation coefficient gives the location of most similar particle pattern in $g(X, Y)$, and the relative position (ΔX, ΔY) shows the displacement of particle image.

$$C_{fg}(\Delta X, \Delta Y) = \sum_{i=1}^{N}\sum_{j=1}^{N} f(X_i, Y_j) g(X_i + \Delta X, Y_j + \Delta Y) \tag{2}$$

$$R_{fg}(\Delta X, \Delta Y) = \frac{\sum_{i=1}^{N}\sum_{j=1}^{N}[f(X_i,Y_j) - f_{\mathrm{m}}][g(X_i + \Delta X, Y_j + \Delta Y) - g_{\mathrm{m}}]}{\sqrt{\sum_{i=1}^{N}\sum_{j=1}^{N}[f(X_i,Y_j) - f_{\mathrm{m}}]^2[g(X_i + \Delta X, Y_j + \Delta Y) - g_{\mathrm{m}}]^2}} \tag{3}$$

Some of the measurement systems apply the fast Fourier Transform (FFT), which shortens the computational time (Raffel, et al., 1998). The distribution of correlation coefficient is obtained by Equations (4) and (5) by means of the FFT operator $\mathscr{F}$

$$S_{fg}(\xi,\eta) = \mathscr{F}^{*}\{f(X,Y)\}\mathscr{F}\{g(X,Y)\} \tag{4}$$

$$C_{fg}(X,Y) = \mathscr{F}^{-1}\{S_{fg}(\xi,\eta)\} \tag{5}$$

The target position and time are also the objective of measurement. The measurement point and time are defined by Equations (6) and (7). In Equation (6), X_0 indicates the location of origin on the image plane, and X_{s} and X_{e} show the starting and ending position of correlation area. The physical location can be obtained by transferring it with magnification factor α. The locations of X_{s} and X_{e} are usually defined by the centre positions of correlation area. The measurement time is defined by the mean value of the pulse time of the laser light sheet as shown by Equation (7), where t_{s} and t_{e} show the first and second pulse time. All the measurement targets u, x, t are the objectives of uncertainty analysis, and they are analysed independently in this procedure.

$$x = \alpha\left[(X_{\mathrm{s}} + X_{\mathrm{e}})/2 - X_0\right] \tag{6}$$

$$t = (t_{\mathrm{s}} + t_{\mathrm{e}})/2 \tag{7}$$

4. MEASUREMENT SYSTEMS

The target experiment and measurement procedure should be clarified before the uncertainty analysis begins. Table 1 shows the principal dimensions of target measurement, which consists of the following sub-systems: (1) Calibration, (2) Flow Visualization, (3) Image Detection, and (4) Data Processing.

4.1 Target flow of measurement.

The target flow field of the present case is a two-dimensional water flow such as the centre plane of a model ship wake. The measurement area is 320 x 330 mm^2, which is determined by the arrangement of camera and optical systems and that also depends on the capacity of laser power for illumination.

4.2 Calibration

The calibration was conducted by insertion of a calibration board at the same position as the laser light sheet. The distance of the reference point l_{r} and its distance on the image plane L_{r} were used to determine the magnification factor, α, as

$$\alpha = l_r \cos\theta / L_r \approx l_r (1-\theta^2/2)/L_r \quad (8)$$

where L_r was obtained by detecting the reference points in pixel units and θ is a small angle between the light sheet and calibration board. This is the simplest method for the calibration.

Target Flow of Measurement		
Target flow		2-D water flow
Measurement facility		Circulating water channel
Measurement area		320 x 330 mm^2
Uniform flow speed		0.5 m/s
Calibration		
Distance of reference points	l_r	260 mm
Distance of reference image	L_r	823 pixels
Magnification factor	α	0.316 mm/pixel
Flow Visualization		
Tracer particle		Spherical nylon particle
Average diameter	d_p	0.05 mm
Standard deviation of diameter	s_p	0.005 mm
Average specific gravity		1.02
Light source		Double pulse Nd:YAG laser
Laser power		20 mJ
Thickness of laser light sheet		1.0 mm
Time interval	Δt	2.4 ms
Image Detection		
Camera		
Spatial resolution		1008 x 1018 pixels
Sampling frequency		30 Hz
Gray scale resolution		8 bit
Cell size		9 µm x 9 µm
Optical system		
Distance from the target	l_t	1100 mm
Length of focus		60 mm
F number of lens		f 2.8
Perspective angle	θ	16.7°
Data Processing		
Pixel unit analysis		Cross correlation method
Correlation area size		32 x 32 pixels
Search area size		16 x 16 pixels
Sub-pixel analysis		3 points Gaussian fitting

Table 1: Principal dimensions of PIV measurement

4.3 Flow visualization.

Spherical nylon particles and laser light sheet were employed for the flow visualization. A double-pulse laser synchronizes to the CCD camera, and the frame straddling technique was applied to shorten the time interval of successive pair images.

4.4 Image detection.

The CCD camera (PIVCAM) recorded the images. It has high-spatial resolution of the captured image and can synchronize to the double-pulse laser. The optical system was designed for optimisation of the quality of the visualized image.

4.5 Data processing.

The direct cross-correlation method was applied in the pixel unit analysis, and it uses the correlation function obtained by Equation (3). A relatively large correlation area was selected for small mis-matching rate, and it affects the lower spatial resolution of the measurement. Three-point Gaussian fitting technique was selected for the sub-pixel analysis. It usually shows stable performance of analysis.

5. DATA FLOW IN MEASUREMENT SYSTEMS

The data flow in the measurement system is shown in Figure 1. The measurement starts from the digital image of the visualized flow field, the pulsing time of illumination, and the distance of reference points. The final targets of the measurement are the flow velocity, the measurement location, and the measurement time. Possible error sources are also shown in Figure 1, and the errors propagate to the final measured target through the data flow.

6. ERROR SOURCES AND PROPAGATION OF ERRORS

6.1 Calibration: α

6.1.1 Calibration board.

Image distance of reference points: L_r

The distance of the reference points were measured on the image plane. If the position of the reference points were detected from a single point of image, the uncertainty band will be 0.5 pixels, and the total amount of uncertainty band will be 0.7 pixels. The sensitivity factor for α will be from Equation (8)

$$\partial\alpha / \partial L_r = -l_r / L_r^2 = -3.84\times10^{-4} \text{ [mm/pixel}^2\text{]}$$

Physical distance of reference points: l_r

The uncertainties of the physical length of the reference points affect the accuracy of the magnification factor. The well-controlled calibration board has less than a 20-µm error. The sensitivity factor of it will be from Equation (8)

$$\partial\alpha / \partial l_r = 1 / L_r = 1.22\times10^{-3} \text{ [1/pixel]}$$

6.1.2 Optical system.

Image distortion: X_s, X_e

The image could be distorted by the aberration of lenses. The distortion of the image affects the error of magnification factor. The distortion of the image will be less than 0.5% of total length, and $0.005L_r = 4.1$ pixel. The sensitivity factor will be given from Equation (8) by

$$\partial\alpha / \partial L_r = -l_r / L_r^2 = -3.84\times10^{-4} \text{[mm/pixel}^2\text{]}$$

Distortion and other error sources of CCD.

The distortion and other error factors from the CCD could cause errors of image detection. The uncertainty band caused by the accuracy of CCD is usually small, and it can be neglected in this case.

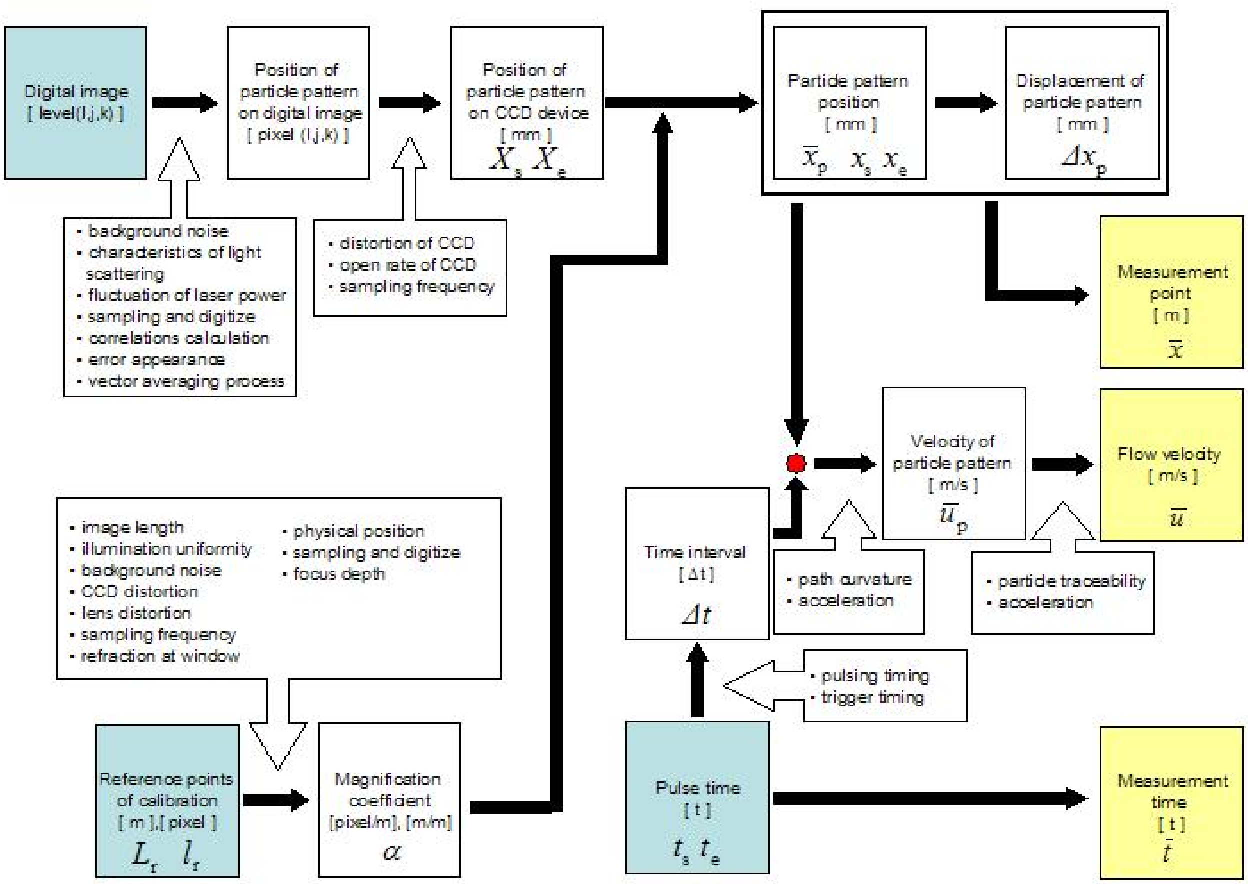

Figure 1: Data flow of PIV measurement

6.1.3 Experimental condition.

Reference board position.

The position of the reference board and the laser light sheet could be different. The difference could affect the accuracy of magnification factor. When the pinhole camera model is assumed, α can be described $\alpha = l_r/L_r = l_t/f$, where l_t and f show the distance from the target and the focus length in pixel unit respectively. The difference is less than Δz_0 = 0.5 mm, and the sensitivity coefficient is obtained as follows because the reduction equation is linear for l_t.

$$\partial\alpha / \partial l_t = l_r / (L_r \cdot l_t) = 2.87 \times 10^{-4} \text{ [1/pixel]}$$

Parallel reference board.

Ideally, the calibration board should be parallel to the laser light sheet for visualization. When the angle between original laser plane and calibration board deviates at most $\theta_1 = 2° = 0.035$ rad from parallel, the sensitivity factor is from Equation (8)
$\partial\alpha / \partial\theta = -l_r \cdot \theta / L_r = -0.011$ [mm/pixel]

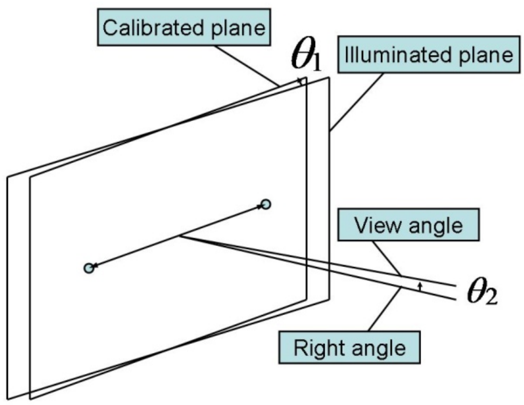

Figure 2: Angles for the calibration board and view

6.2 Displacement of Particle Image: ΔX

6.2.1 Visualization.

Laser power fluctuation

The spatial and temporal fluctuation of laser power could affect on the detection of particle image position directly. The maximum uncertainty could be in the length of particle diameter. If the experimental condition is well controlled, uncertainty can be reduced to 1/10 of particle diameter. The displacement of the particle is obtained from two particle images, and the uncertainty band could be estimated as $\Delta x = 7.1 \times 10^{-3}$ mm, and the sensitivity factor is from Equation (6)
$\partial X / \partial x = 1/\alpha = 3.16$ [pixel/mm].

6.2.2 Image detection.

Optical system

The distortion of image cased by lens aberration could affect the detection of particle position. However, this factor is already accounted as the error of magnification factor, and it will not be change through the measurement.

CCD distortion

The CCD distortion is the same error source with one in the calibration of the optical system, and the amount of error could be 0.0056 pixels. The error may be different cell by cell, and then the error should take into account here again. The sensitivity factor is from Equation (6)
$\partial x / \partial X = \alpha = 0.316$.

Normal view angle.

The normal or perpendicular view angle to the illumination plane could affect the uncertainty of the displacement. The angle could be estimated as $\theta_2 = 2°$, and the sensitivity factor is
$\partial\alpha / \partial\theta = -l_r \cdot \theta / L_r = -0.011$ [mm/pixel].

6.2.3 Data processing.

Mis-matching error.

In the pixel unit analysis, mis-matching of pair particle images could happen. Large serious error can be detected by comparing the candidate vector with surrounding ones, but small errors of mis-matching cannot be detected usually. The possibility of the error can be considered by means of an artificial image (Okamoto, et al., 2000, Nishio, et al., 2003), which enables detection of the measurement error directly. The uncertainty band of the pixel unit analysis could be estimated statistically, and it could be about 0.2 pixels.

Sub-pixel analysis.

The uncertainties of sub-pixel analysis depend on many factors such as the diameter of tracer particle, noise level of the image, and particle concentration. The system error of sub-pixel analysis can be estimated by means of standard image (Okamoto et at, 2000), and it could be about 0.03 pixels.

Other error sources may exist, which affect the results of image analysis, but those effects can be regarded as the indirect procedure. They may be included in the error rate of image analysis.

6.3 Time Interval: *Δt*.

6.3.1 Delay generator.

The delay generator controls the pulse timing, and the possible fluctuation will be 2 ns, which is obtained from the user manual. The sensitivity factor for the measurement time is 1.

6.3.2 Pulse timing accuracy.

The pulse laser itself has an uncertainty for the pulse timing. The uncertainty band for it will be 5 ns, which obtained form manual. The sensitivity factor for the measurement time is 1.

6.4 Experiment: δu.

6.4.1 Particle trajectory

The particle trajectory depends on the acceleration of flow field, and the tracer particles for liquid flow have usually very low velocity lag from acceleration of the fluid (Raffel, et al. 1998). When the particle diameter is 50 μm and the relative density is 1.02, nearly neutrally buoyant, the error from velocity lag is less than 0.01% of total velocity. Then in this case,
$\delta u = 0.5 \times 1000 \times 0.0001 = 0.5\,\text{mm/s}$

6.4.2 Three-dimensional effects on perspective of velocity

The perspective of out-of-plane velocity component affects the in-plane measured value. The measured velocity can be described as follows:

$$u_m = u + w \cdot \tan\theta \qquad (9)$$

where w is the normal velocity component. Then $w \cdot \tan\theta$ indicates the error component. The perspective angle θ can be estimated by the distance from the target plane and the size of measurement area. When the out of plane component of velocity is assumed as 1.0% of uniform flow, the error could be estimated as

$500 \times 0.01 \times \tan(160/1100) = 0.73$ [mm/s]

6.5 Measurement position: *x*

6.5.1 Centre position of correlation area: X_s, X_e.

The centre position of correlation area is defined in pixel units, and it has at most 0.5 pixels uncertainty. The sensitivity coefficient is from Equation (6)
$\partial x / \partial X = \alpha = 0.316$ [mm/pixel].

6.5.2 Non-uniformity of tracer particle distribution.

The flow speed is identified from the displacement of a particle image. When the particle distribution is not uniform in the correlation area, the centre position of the measured velocity field could be apart from the centre of correlation area. The possibility of the bias will be at most one fourth of the correlation area size, and the sensitivity factor is from Equation (6) $\partial x / \partial X = \alpha = 0.316$ [mm/pixel].

6.5.3 Origin correlation.

The X_0 indicates the location of the origin on the image plane. The correlation between physical space and image plane should be identified for the definition of the coordinate system. The correlation could have uncertainty in the range of 2 pixels, and the sensitivity factor is from Equation (6) $\partial x / \partial X = \alpha = 0.316$ [mm/pixel].

6.5.4 Magnification factor.

The coordinates of each measurement point are obtained by transferring the image position to physical space by Equation (6). The magnification factor appeared in Equation (6) has an uncertainty as described in Section 6.1. The sensitivity factor for the position is from Equation (6)

$\partial x / \partial \alpha = X$ [pixel],

and it can be selected as the half-length of the image width.

6.6 Measurement time: *t*

The fluctuation of pulse time could be an error source of measurement from the time series analysis. The measurement time is defined by Equation (7), and the uncertainties of t_s and t_e are the same as Δt as described in Section 6.3.

7. SUMMARY OF UNCERTAINTIES

The uncertainties of measurement were summarized in Table 2 and Table 3. Root-sum-square is employed for the accumulation of uncertainties. Table 2 summarizes the propagation and accumulation of uncertainties for measurement parameters α, ΔX, Δt, δu, and the final measurement target velocity u. The uncertainty propagation to the measurement target position x and time t is also considered as shown in Table 3. The uncertainties of u, x, and t are analysed independently. When accumulation for total performance of the measurement system by the uncertainty for the flow speed is needed, the following summation can be applied, where u_u, u_x, and u_t represent the uncertainties of u, x, and t, respectively:

$$u_c = \sqrt{u_u^2 + (u_x \partial u / \partial x)^2 + (u_t \partial u / \partial t)^2} \quad (10)$$

When the combined uncertainties are considered, the major uncertainty sources may be evaluated. The largest uncertainty source in this case is the mis-matching uncertainty of ±0.20 pixels, which appeared in the image analysis procedure. Its contribution to the uncertainty in velocity is ±26 mm/s in comparison to the combined uncertainty for all elements of ±27 mm/s. The next two largest sources are the sub-pixel analysis, ±0.03 pixels or ±4.0 mm/s, and the uncertainty of calibration caused by the lens aberration, ±4.11 pixels or ±2.5 mm/s. This kind of analysis can contribute to the improvement of measurement systems. For this example, any significant improvement in uncertainty must focus on the mis-matching error. For the uniform flow, the expanded uncertainty in velocity is (0.500 ±0.054) m/s or ±11 % for a coverage factor of 2.

Parameter	Category	Error sources	$u(x_i)$	(unit)	c_i	(unit)	$c_iu(x_i)$	u_c.
α (mm/pix)	Calibration	Reference image	0.70	(pix)	3.84E-04	(mm/pix^2)	2.69E-04	
		Physical distance	0.02	(mm)	1.22E-03	(1/pix)	2.44E-05	
		Image distortion by lens	4.11	(pix)	3.84E-04	(mm/pix^2)	1.57E-03	
		Image distortion by CCD	0.0056	(pix)	3.84E-04	(mm/pix^2)	2.15E-06	
		Board position	0.5	(mm)	2.84E-04	(1/pix)	1.42E-04	
		Parallel board	0.035	(rad)	0.011	(mm/pix)	3.85E-04	0.00165
ΔX (pix)	Acquisition	Laser power fluctuation	0.0071	(mm)	3.16	(pix/mm)	.0224	
		Image distortion by CCD	0.0056	(pix)	1.0		0.0056	
		Normal view angle	0.035	(rad)	0.011	(mm/pix)	3.85E-04	
	Reduction	Mis-matching error	0.20	(pix)	1.0		0.20	
		Sub-pixel analysis	0.03	(pix)	1.0		0.03	0.204
Δt (s)	Acquisition	Delay generator	2.00E-09	(s)	1.0		2.00E-09	
		Pulse time	5.00E-09	(s)	1.0		5.00E-09	5.39 E-09
δu (mm/s)	Experiment	Particle trajectory	0.05	(mm/s)	1.0		0.050	
		3-D effects	0.73	(mm/s)	1.0		0.73	0.732

Parameter	Category	Error sources	$u(x_i)$	(unit)	c_i	(unit)	$c_iu(x_i)$	(unit)
α		Magnification factor	0.00165	(mm/pix)	1580.0	(pix/s)	2.61	
ΔX		Image displacement	0.204	(pix)	132.0	(mm/ pix/s)	26.8	
Δt		Image interval	5.39E-09	(s)	1.2	(mm/s^2)	6.47E-09	
δu		Experiment	0.732	(mm/s)	1.0		0.732	
			Combined uncertainty		u_u		26.9	(mm/s)

Standard uncertainty: $u(x_i)$ Combined uncertainty: u_c

Sensitivity coefficient: $c_i = \partial f / \partial x_i$

Table 2: Summary of uncertainties for velocity u

Parameter	Category	Error sources	$u(x_i)$ (unit)	c_i (unit)	$c_i u(x_i)$ (unit)
X_s, X_e	Acquisition	Digital error	0.5 (pix)	0.316 (mm/pix)	0.158
		Non-uniformity of distribution	8.0 (pix)	0.316 (mm/pix)	2.53
X_0	Calibration	Origin correlation	2.0 (pix)	0.316 (mm/pix)	0.632
α		Magnification factor	0.00178 (mm/pix)	506.0 (pix)	0.906
			Combined uncertainty	u_x	2.76 (mm)

Parameter	Category	Error sources	$u(x_i)$ (unit)	c_i (unit)	$c_i u(x_i)$
t_s, t_e	Acquisition	Delay generator	2.00E-09 (s)	1.0	2.00E-09
		Pulse time	5.00E-09 (s)	1.0	5.00E-09
			Combined uncertainty	u_t	5.39E-09 (s)

Standard uncertainty: $u(x_i)$

Sensitivity coefficient: $c_i = \partial f / \partial x_i$

Table 3: Summary of uncertainty for position, *x*, and time, *t*

8. LIST OF SYMBOLS

C_{fg}	Covariance function of particle images *f* and *g*, Equation (2)	
c_i	Sensitivity coefficient, $c_i = \partial f / \partial x_i$	
d_p	Particle diameter	mm
$\mathcal{F}$	Fourier transform operator	
f	Initial set of particle images	
g	Second set of particle images	
L_r	Distance of reference image	pixel
l_r	Distance of reference point	mm
l_t	Distance from target to lens	mm
R_{fg}	Cross-correlation function particle images of *f* and *g*, Equation (3)	
S_{fg}	Spectrum of particle images f and g, Equation (4)	
s_p	Standard deviation of particle diameter	mm
t	Time	s
t_e	End time on second laser pulse	s
t_s	Start time on first laser pulse	s
u	Standard uncertainty	
u	Fluid velocity in axial direction, *x*	mm/s
w	Fluid velocity in vertical direction	mm/s
X	Axial coordinate of particle in image plane	
X_e	End location of particle	pixel
X_s	Start location of particle	pixel
x	Location of fluid particle in physical plane	mm
Y	Vertical coordinate of particle in image plane	pixel
α	Magnification factor	mm/pixel
θ	Viewing angle	rad

9. REFERENCES

Adrian, R. J., 1986, "Image Shifting technique to resolve directional ambiguity in double-pulsed velocimetry," Applied Optics, 25, pp. 3855-3858.

Keane, R. D. and Adrian, R. J., 1991, "Optimization of Particle Image Velocimeters. Part II: Multiple Pulse Systems," Measurement Science and Technology, 2, pp. 1202-1215.

Nishio, S., Okamoto, K., Kobayashi, T., and Saga, T., 1999, "Evaluation of System Performance and Uncertainty Analysis of PIV (PIV-STD Project)," Proceedings of the 3rd International Workshop on Particle Image Velocimetry, pp. 465-470.

Nishio, S. and Murata, S., 2003, "A Numerical Approach to the Evaluation of Error Vector Appearance Possibility in PIV," Proceedings of 5th International Symposium on Particle Image Velocimetry, pp. 3321.1-3321.9.

Okamoto, K., Nishio, S., Saga, T., and Kobayashi, T., 2000, "Standard Images for Particle Image Velocimetry," Journal of Measurement Science and Technology, Institute of Physics, Vol. 11, No. 6, pp. 685-691.

Raffel, M., Willert, C., and Kompenhans, J., 1998, Particle Image Velocimetry: A Practical Guide, Berlin: Springer-Verlag.

Visualization Society of Japan, 2002, Handbook of Particle Image Velocimetry, Morikita Publishing Co. Ltd. (in Japanese).